BATTERY AND SUPERCAPACITOR CHARGER BASED ON LLC CONVERTER

Dorin PETREUŞ, Toma PĂTĂRĂU, Ionuț CIOCAN
Technical University of Cluj-Napoca, Faculty of Electronics, Telecommunications and Information Technology, 26-28 G. Barițiu Street, 400027 Cluj-Napoca, Romania, Phone +40264401415, E-mail: Dorin.Cadar@ael.utcluj.ro

Abstract: The need for a small economical power supply for battery chargers has increased in the last couple of years. A LLC converter can be used as a battery charger due to its low EMI noise, high power integration and high efficiency. The paper presents a more accurate approach for the design and analysis of the LLC converter. A comparison between the calculations, the simulations and the practical results is also presented. A new analysis and design method which enables the use of the LLC converter as a battery charger and super capacitor charger is presented.

Keywords: *resonant converters, battery charger, ZVT, ZCT.*

I. INTRODUCTION

Energy storage systems like battery and Super Capacitors became more and more important in the last couple of years. The development of an efficient battery charger circuit which produces a very low amount of EMI noise is one of the main concerns of research nowadays.

The growing popularity of the LLC converter in its half-bridge implementation is due to its high efficiency, low EMI emission and the ability to achieve high power integration.

A LLC converter has many advantages over the other resonant topologies. It can regulate the output voltage over a wide range of load and input voltage variations. It can obtain zero voltage switching over the entire operating range. In many papers [1], [2] the first harmonic approximation is used because it enables the analysis of the LLC converter by means of classical AC circuit analysis.

The first harmonic approximation considers the circuit as a band pass filter with square wave excitation. The method consists of replacing the square wave input signal with its fundamental value [3]. In [1-3] a first harmonic model of the converter is derived and the design method is based then on this model.

This paper presents a more accurate approach for the analysis and design of a LLC converter.

The resonant tank of the converter consists of three reactive elements: resonant capacitance C_r, resonant inductor L_r and the magnetizing inductance of the transformer L_p. As demonstrated in [4], [5] there are two resonant frequencies: one determined by the resonant capacitor C_r and resonant inductor L_r and the other one determined by the resonant capacitor and the magnetizing inductance of the transformer L_p in series with the resonant inductance.

$$f_r = \frac{1}{2\pi\sqrt{C_r L_r}} \tag{1}$$

$$f_p = \frac{1}{2\pi\sqrt{C_r (L_r + L_p)}} \tag{2}$$

The converter can work in three fundamental operating modes: $f < f_p$, $f_p < f < f_r$, $f > f_r$.

The converter is designed to work always in the inductive region because in the capacitive mode a large voltage develops across the resonant capacitor thus a large energy level must be circulating in the resonant tank [6]. The converter must work always in the inductive region below f_r, $f_p < f < f_r$. In this region the converter can achieve zero voltage switching (ZVS) for the MOSFETS and zero current switching (ZCS) for the diodes in the rectifier network for the entire operating range [6], [7].

To do this the converter should work at the resonant frequency at nominal input voltage and full load. At light load the characteristic of a SRC is dominant and at full load the characteristics of a PRC comes on top [8].

The gain characteristic of a LLC converter is presented in Figure 1.

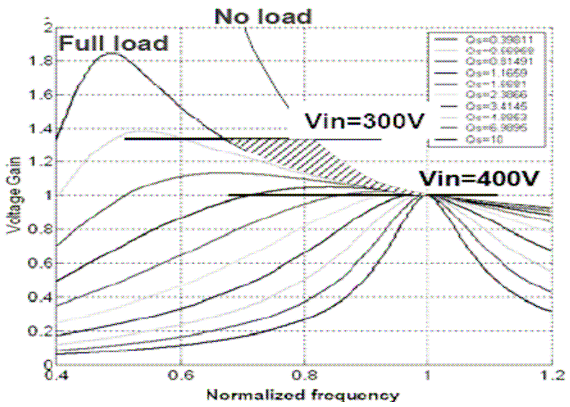

Figure 1. Characterictic of a LLC converter.

Manuscript received April 16, 2010; revised June 2, 2010

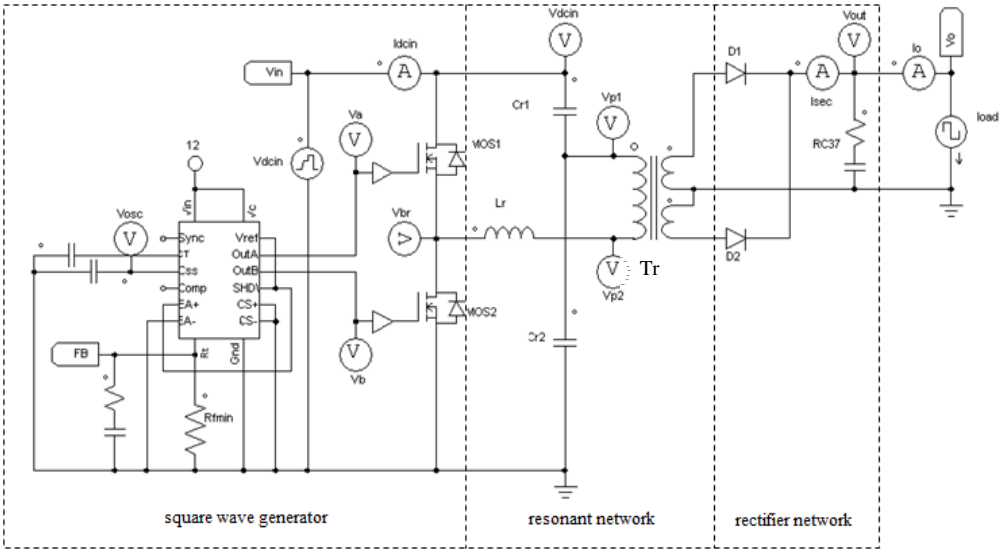

Figure 2. Schematic of The LLC converter

From Figure 1 one can easily see that at the second resonant frequency the gain is independent of the load [9].

These properties enable the use of the LLC converter in battery and super capacitor charger applications.

This paper presents a new and more accurate method for the analysis of the resonant converter. First the method is described then the results obtained are compared with the ones from simulations and the ones from the practical design.

II. CONVERTER OPERATING PRINCIPLES AND DESIGN

The proposed circuit is presented in Figure 2. The LLC converter consists of three important stages: square wave generator, resonant tank and rectifier network.

The functionality of the LLC converter can be divided in four stages. The equivalent circuits as seen from the primary side of the four stages are presented in Figure 3.

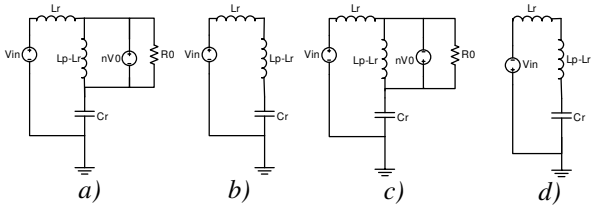

Figure 3. Functional stage: a) for the interval 0 – $T_r/2$, b) for the interval $T_r/2$ - T_w c)for the interval T_w - T_w+ $T_r/2$, d) for the interval T_w+ $T_r/2$ - T_w.

T_r represents the resonant period and T_w is the switching period.

Because the resonant frequency f_p is small enough for *b)* and *d)* cases the inductor current will be considered constant.

The characteristic impedance Z_0 of the resonant tank is:

$$Z_0 = \sqrt{\frac{L_r}{C_r}} \tag{3}$$

The equivalent load resistance R_{ac} as seen from the primary side can be calculated with [1]:

$$R_{ac} = \frac{8n^2}{\pi^2} R_0 \tag{4}$$

were n is the transformer turns ratio and R_0 is the output load.

The quality factor Q is:

$$Q = \frac{Z_0}{R_{ac}} \tag{5}$$

The gain of the LLC converter can be expressed as [1]:

$$M(f,m,Q) = \left| \frac{\left(\frac{f}{f_r}\right)^2 (m-1)}{\left(\frac{f^2}{f_p{}^2} - 1\right) + j\frac{f}{f_r}\left(\frac{f^2}{f_r{}^2} - 1\right)(m-1)Q} \right| \tag{6}$$

where m represents the ratio of the: $m = L_m/L_r$.

The gain characteristic of the LLC converter described by (6) is presented in Figure 4.

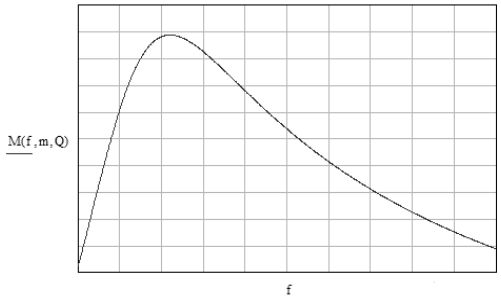

Figure 4. Gain characteristic of the LLC converter.

The magnetizing current of the transformer I_M reaches its maximum value at a quarter of the resonant period and is:

$$I_M = \frac{n \cdot V_0}{(L_p - L_r)}\left(\frac{T_r}{4}\right) \tag{7}$$

were V_0 is the output voltage of the converter.

Considering the four stages described in Figure 3 the magnetizing current is defined over the entire period as follows:

$$i_m(t) = \begin{cases} \left(-I_M + \dfrac{nV_0}{L_p - L_r}t\right) & if \quad 0 \le t \le \dfrac{T_r}{2} \\ I_M \quad if \quad \left(\dfrac{T_r}{2}\right) \le t \le \dfrac{1}{2f_{sw}} \\ I_M - \dfrac{nV_0}{L_p - L_r}\left(t - \dfrac{1}{2f_{sw}}\right) & if \quad \dfrac{1}{2f_{sw}} \le t \le \dfrac{1}{2f_{sw}} + \dfrac{T_r}{2} \\ -I_M \quad if \quad \dfrac{1}{2f_{sw}} + \dfrac{T_r}{2} \le t \le \dfrac{1}{f_{sw}} \end{cases} \tag{8}$$

were $i_m(t)$ represents the magnetizing current and f_{sw} is the switching frequency of the square wave generator.

The magnetizing current described by (8) is represented in Figure 5:

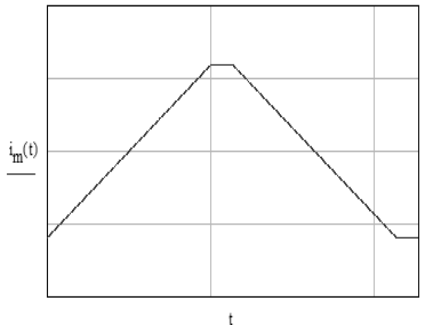

Figure 5. Magnetizing current.

The current through the resonant inductor if the magnetizing current is considered zero is given by:

$$I_s = \frac{I_{av}}{n \cdot \eta}\frac{\pi}{2}\frac{1}{f_{sw} \cdot T_r} \tag{9}$$

where: $\eta = P_{out}/P_{in}$.

The phase between the two currents is:

$$\theta = \arctan\left(\frac{I_M}{I_S}\right) \tag{10}$$

The current through the resonant inductor for half of the resonant period, *[0 - T_r /2]*, considering the magnetizing current also sinusoidal, is:

$$i_L(t) = \sqrt{I_S{}^2 + I_M{}^2}\,\sin(\omega_r t - \theta) \tag{11}$$

Substituting (9) and (10) in (11) and considering the entire period, one can express the resonant inductor current as:

$$i_{Lt}(t) = \begin{cases} \sqrt{I_S{}^2 + I_M{}^2}\,\sin\left(\dfrac{t}{\sqrt{L_r C_r}} - \theta\right) & if \quad 0 \le t \le \dfrac{T_r}{2} \\ I_M \quad if \quad \dfrac{T_r}{2} \le t \le \dfrac{1}{2f_{sw}} \\ -\sqrt{I_S{}^2 + I_M{}^2}\,\sin\left(\dfrac{t - \dfrac{1}{2f_{sw}}}{\sqrt{L_r C_r}} - \theta\right) & if \quad \dfrac{1}{2f_{sw}} \le t \le \left(\dfrac{1}{2f_{sw}} + \dfrac{T_r}{2}\right) \\ -I_M \quad if \quad \left(\dfrac{1}{2f_{sw}} + \dfrac{T_r}{2}\right) \le t \le \dfrac{1}{f_{sw}} \end{cases} \tag{12}$$

where $i_{Lt}(t)$ is the resonant current over the entire period.

The resonant inductor current derived from (12) is represented in Figure 6.

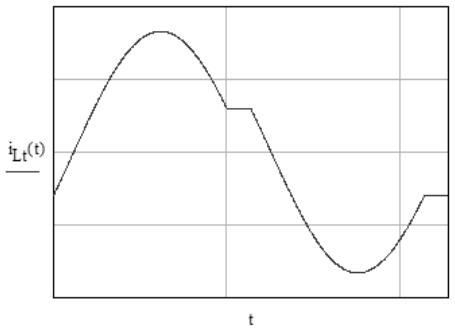

Figure 6. Resonant inductor current.

The RMS value of the resonant current I_{Lrms} is:

$$I_{Lrms}(t) = \sqrt{f_{sw}\int_0^{\frac{1}{f_{sw}}}\left(i_{Lt}(t)^2\right)dt} \tag{13}$$

The current through one transistor can be easily determined if one considers that the transistor will be on only one half of the switching period T_w.

$$i_T(t) = \begin{cases} \sqrt{I_S{}^2 + I_M{}^2}\,\sin\left(\dfrac{t}{\sqrt{L_r C_r}} - \theta\right) & if \quad 0 \le t \le \dfrac{T_r}{2} \\ I_M \quad if \quad \dfrac{T_r}{2} \le t \le \dfrac{1}{2f_{sw}} \\ 0 \quad if \quad \dfrac{1}{2f_{sw}} \le t \le \dfrac{1}{f_{sw}} \end{cases} \tag{14}$$

where $i_T(t)$ represents the transistor current.

The transistor current described by (14) is represented in Figure 7. The transistor current is null for a half of the switching cycle. Because the circuit is working in the

inductive region the current at the beginning of the switching cycle is negative.

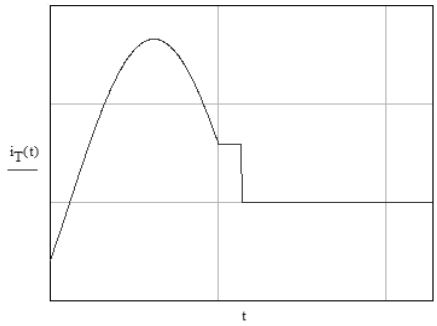

Figure 7. Transistor current.

The RMS value of the transistor I_{Trms} is given bylated as:

$$I_{Trms}(t) = \sqrt{f_{sw} \int_0^{\frac{1}{f_{sw}}} \left(i_T(t)^2\right) dt} \quad (15)$$

Because the LLC converter can achieve zero voltage switching on the entire input range the switching losses are zero. The conduction loss of the transistor is:

$$P_T = R_{DSon} \cdot I_{Trms}^{\ 2} \quad (16)$$

where R_{DSon} is the on resistance of the transistor.

The junction temperature of the diode can be calculated as:

$$T_{JT} = T_A + R_{thJA} \cdot P_T \quad (17)$$

were T_{JT} is the junction temperature of the MOSFET transistor, T_A is the ambient temperature and R_{thJA} is the thermal junction to ambient resistance of the transistor.

The current through the rectifier diodes can be expressed as the difference between the resonant current and the magnetizing current:

$$i_{D1}(t) = n \cdot \eta \cdot (i_{Lt}(t) - i_m(t)) \quad (18)$$

The current through both diodes is shown in *Figure 8.*

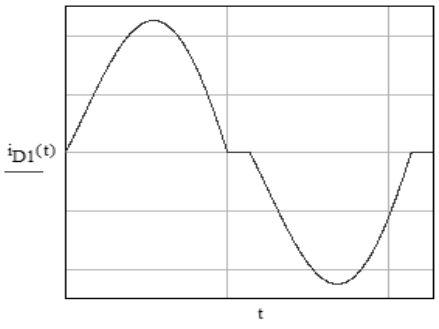

Figure 8. Diode current.

The average current through the output diode is:

$$I_{av} = 2 \cdot f_{sw} \int_0^{\frac{T_r}{2}} n \cdot \eta \cdot (i_{Lt}(t) - i_m(t)) dt \quad (19)$$

The RMS value of the diode current is:

$$I_{rmsd} = \sqrt{2 \cdot f_{sw} \int_0^{\frac{T_r}{2}} [n \cdot \eta \cdot (i_{Lt}(t) - i_m(t))]^2 dt} \quad (20)$$

Considering the currents calculated in (18) and (19) the power loss due to the diode can be expressed as:

$$P_D = V_F \cdot I_{av} + r_d \cdot I_{rmsd}^{\ 2} \quad (21)$$

where V_F is the forward voltage drop and r_d the on resistance of the diode.

The calculated power is used to determine the type of diode used and can also be used to determine the maximum junction temperature.

The junction temperature of the diode can be calculated with:

$$T_{JD} = T_A + R_{thJA} \cdot P_D \quad (22)$$

where T_{JD} is the junction temperature of the diode, R_{thJA} is the junction to ambient thermal resistance of the diode and T_A represents the ambient temperature.

A theoretical method for charging a battery or a supercapacitor can be to implement a charging algorithm in two steps, as in Figure 9 [10].

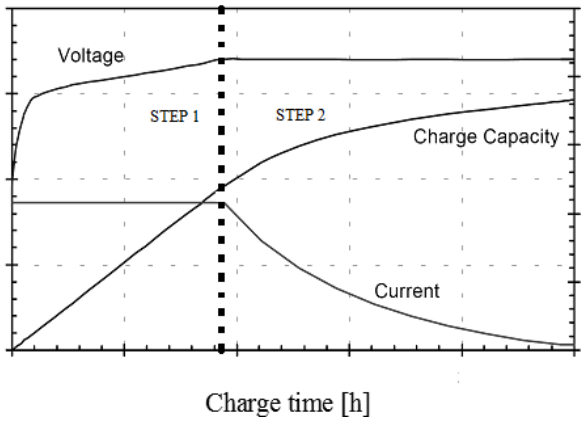

Figure 9. Battery charge characteristic

The battery/supercapacitor is charged first with a constant current, supplied to the battery until the voltage reaches a threshold given by the producer of the battery/ supercapacitor. In the second step, the voltage on the battery/supercapacitor is kept constant until the current drops below a threshold value which is prescribed by the designer. This threshold is usually 0.05C for common batteries.

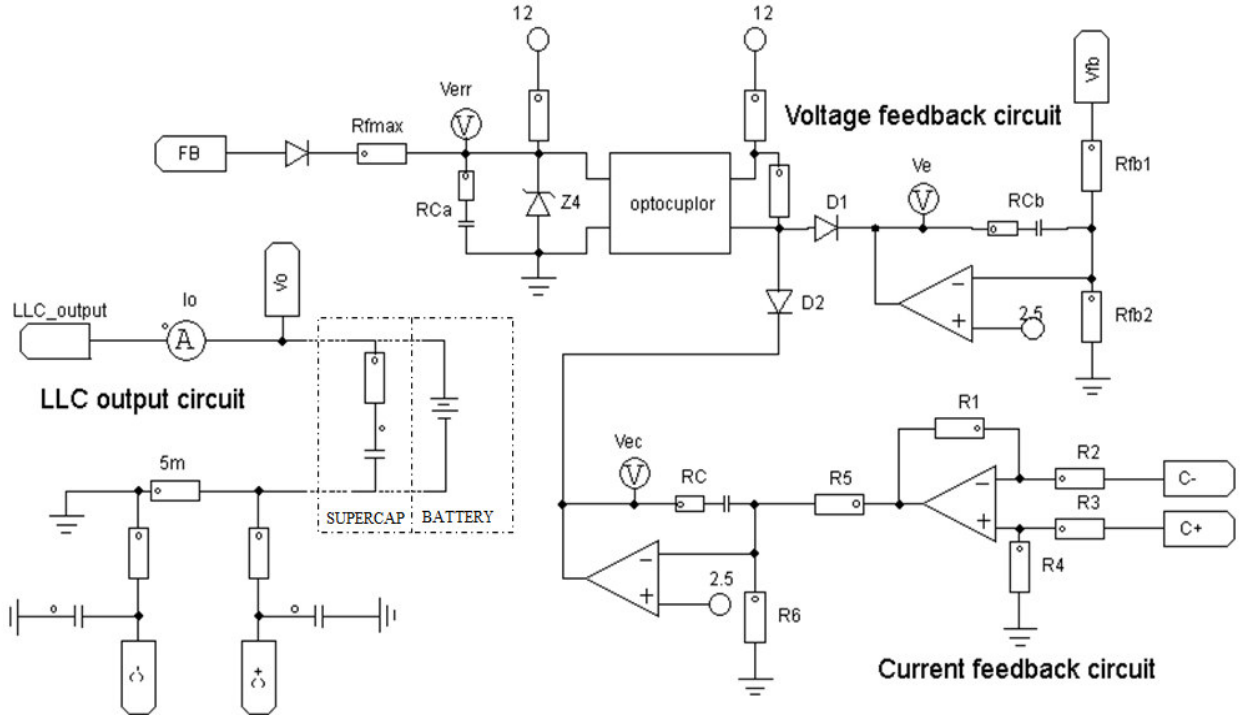

Figure 10. Control circuit.

The control circuit is designed to keep the current constant when the voltage of the battery or super capacitor is below the prescribed value, step 1, and to keep the voltage constant when the battery/supercapacitor voltage threshold is reached, step 2.

When the output current of the LLC converter is lower than the prescribed current of the loop D2 is off, D1 is on and the converter works as a constant voltage source. In this mode the voltage loop regulates the output voltage and the current loop is disabled. When the current is larger than the current prescribed diode D1 is off D2 is on and the converter works as constant current source. In this mode the current loop keeps the current constant and the voltage loop is disabled.

An optocoupler is used to ensure galvanic separation between the input and the output of the LLC converter end to satisfy the safety standards for electrical security.

This feature together with the ability to achieve high power integration and high efficiency enable the use of the LLC converter as a battery charger and also a super capacitor charger.

III. SIMULATION RESULTS OF THE CONVERTER

A simulation model for the LLC converter was build with the following input parameters: V_{out} = 12V, I_{out} = 12.5A, P_{out}= 150W. The calculated values for the resonant tank are: L_r = 269uH, L_p = 1079uH, C_r =9.4nF.

The magnetizing current calculated with (8) for V_{in} = 350V, is presented in MathCad
Figure *11* a), together with PSIM simulation
Figure *11* b).

As one can seen from
Figure *11*, the circuit is working below the second resonant frequency f_r and even if the magnetizing current is considered constant from T_r to T_{sw} the approximation is very close to the simulation result.

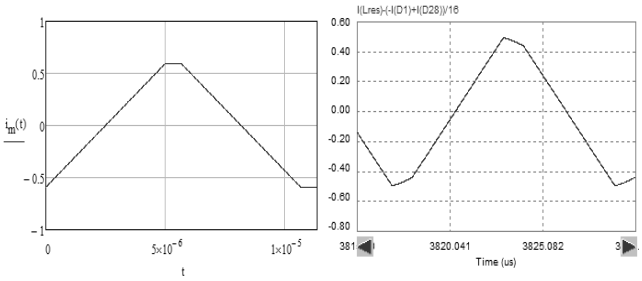

a) *b)*

Figure 11. Magnetizing current: a) MathCad, b) PSIM

Considering V_{in} = 400V The magnetizing current is obtained as represented in Figure 12.

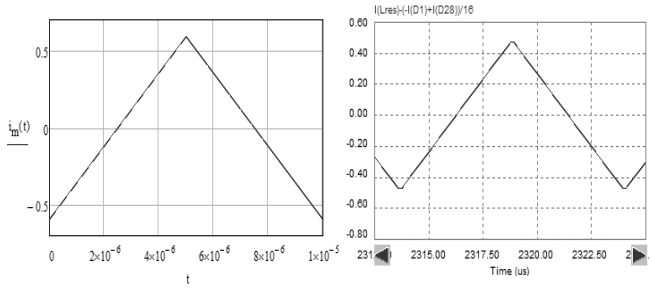

a) *b)*

Figure 12. Magnetizing current: a) MathCad; b) PSIM.

The resonant current obtained representing (12) for the designed converter in MathCad is presented in Figure 13 a)

together with the PSIM simulation results Figure 13 b). The results are obtained for V_{in} =350V.

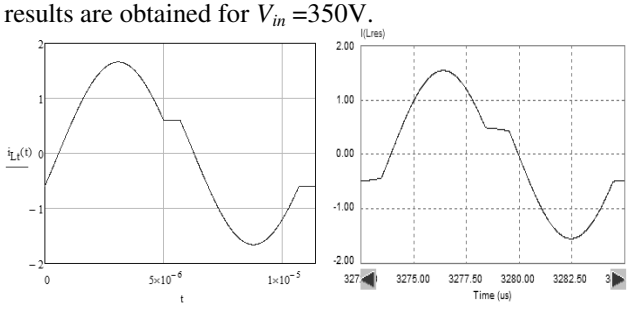

a) *b)*

Figure 13. Resonant current: a) MathCad; b) PSIM.

Considering V_{in} = 400V The resonant current is obtained as represented in Figure 14.

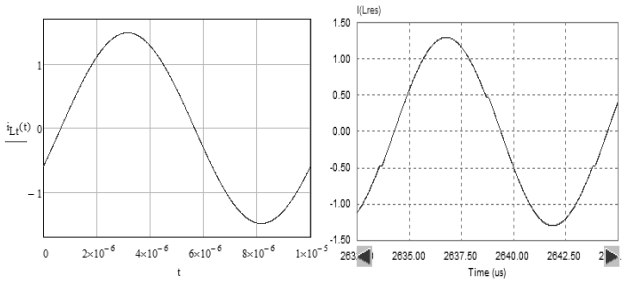

a) b)

Figure 14. Resonant current: a) MathCad; b) PSIM.

The current through the MOSFET obtained representing (14) for the designed converter in MathCad is presented in Figure 15 a), together with the PSIM simulation results, in Figure 15 b). The results are obtained for V_{in} = 350V.

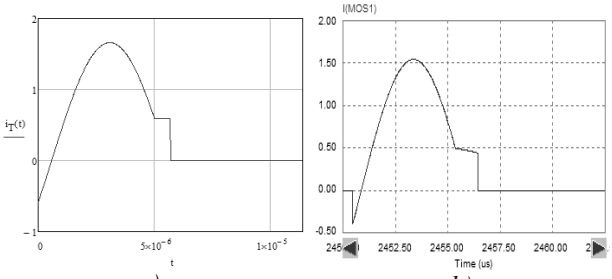

a) *b)*

Figure 15. Transistor current: a) MathCad; b) PSIM.

Considering V_{in} = 400V The MOSFET current is obtained as represented in *Figure 16.*

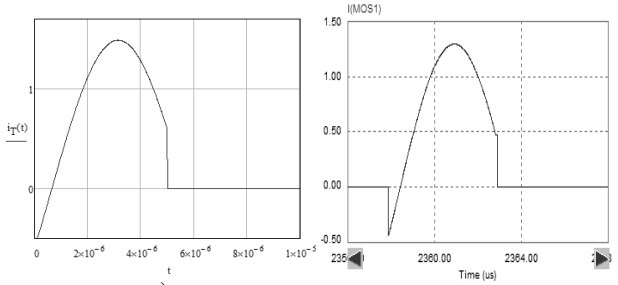

a) b)

Figure 16. Transistor current: a) MathCad; b) PSIM.

The current through the diodes obtained representing (18) for the designed converter in MathCad is presented in Figure 17, together with the PSIM simulation results.

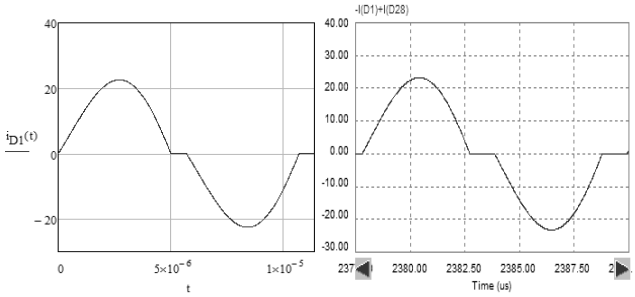

a) *b)*

Figure 17. Diodes Current: a) MathCad; b) PSIM.

Considering V_{in} = 400V the MOSFET current is obtained as represented in *Figure 18.*

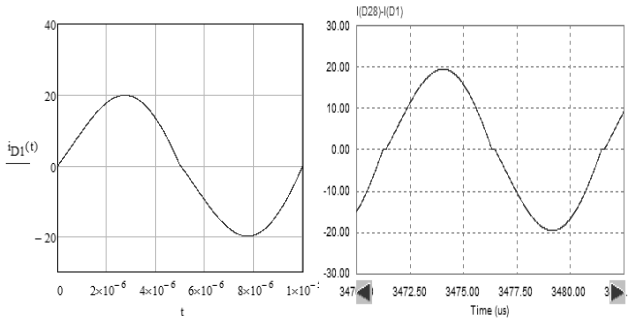

a) *b)*

Figure 18. Diodes Current: a) MathCad, b) PSIM

The characteristic of the charger is presented in Figure 19. The charger keeps the current constant until the voltage is 12V and then the current drops to 0 and the voltage is kept constant.

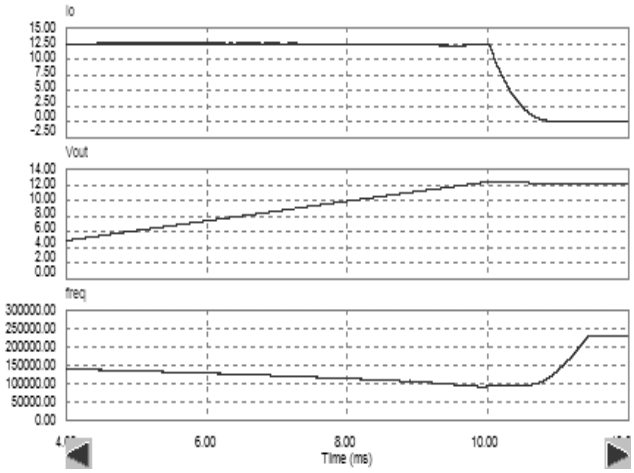

Figure 19. Charger characteristic.

IV. MEASUREMENTS

A LLC converter with the following parameters was realized: : V_{out} = 12V, I_{out} = 12.5A, P_{out}= 150W.

The waveform for the resonant current considering V_{in} = 350V is represented in Figure 20 a) and for V_{in} = 400V in Figure 20 b).

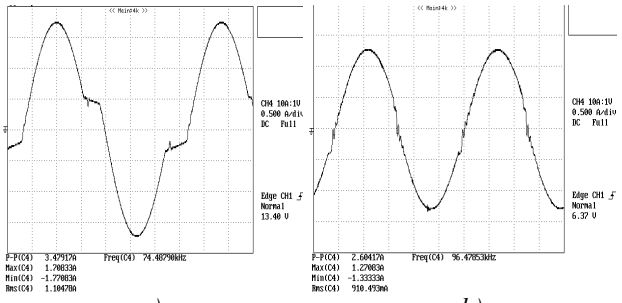

a) *b)*

Figure 20. Resonant current.

The waveform for the resonant current considering V_{in} = 350V is represented in Figure 21 a) and for V_{in} = 400V in Figure 21 b).

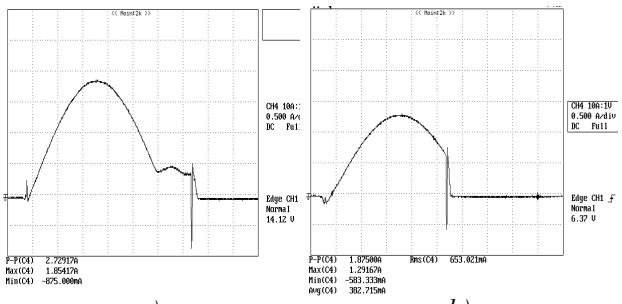

a) *b)*

Figure 21. Transistor current.

The waveform for the resonant current considering V_{in} = 350V is represented in Figure 22 a) and for V_{in} = 400V in Figure 22 b).

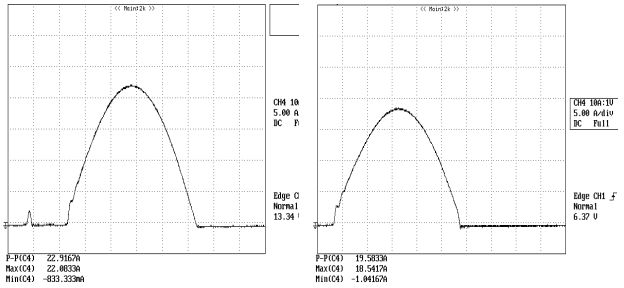

a) *b)*

Figure 22. Diode current.

V. CONCLUSIONS

The paper presents a method for the design and analysis of a battery charger based on a LLC converter. The LLC converter is suited for battery charger applications due to its low EMI emission and the ability to achieve high power integration and high efficiency.

In many papers the first harmonic approximation is used for the design of the converter because it enables the analysis of the LLC convertor by means of classical AC circuit analysis. This paper presents a more accurate method for the design and analysis of the LLC converter.

The simulation end experimental results validate the proposed method. The proposed control method of the LLC converter enables the use of the converter as a battery charger, and also as a supercapacitor charger.

ACKNOWLEDGEMENT

This work was supported by CNCSIS – UEFISCSU, project number 79/1.10.2007 of the PNII – IDEI ID_1019/2007 program.

REFERENCES

[1] Fairchild Semiconductor Corp., "Half-Bridge LLC Resonant Converter Design Using FSFR-series Fairchild Power Switch", Appl. Note 4151, pp. 1-17, 2007.

[2] STMicroelectronics, "LLC Resonant Half-bridge Converter Design Guideline", Appl. Note 2450, pp. 1-32, 2007.

[3] ON Semiconductor, "A Simple DC SPICE Model for the LLC Converter", Appl. Note 8255D, pp. 1-12, 2006.

[4] Mingping Mao, Dimitar Tchobanov, Dong Li, Martin Maerz, Tobias Gerber, Gerald Deboy, Leo Lorenz, "Analysis and Design of a 1MHz LLC Resonant Converter with Coreless Transformer Driver", *International Conference & Exhibition for Power Electronics*, China, 2007.

[5] ON Semiconductor, "Understanding the LLC Structure in Resonant Applications", Appl. Note 8311D, pp. 1-16, 2008.

[6] STMicroelectronics, "An Introduction to LLC Resonant Half Bridge Converter", Appl. Note 2644, pp. 1-64, 2007.

[7] Yu Fang, Dehong Xu, Yanjun Zhang, F. Gao, L. Zhu, "Design of High Power Density LLC Resonant Converter with Extra Wide Input Range", *The 22nd Annual Applied Power Electronics Conference and Exposition*, Australia, pp. 976-981, 2007.

[8] Bo Yang, "Topology Investigation for Front End DC/DC Power Conversion for Distributed Power System", Ph.D. thesis, Virginia Polytechnic Institute and State University, Blacksburg, Virginia, 2003.

[9] Ya Liu, "High Efficiency Optimization of LLC Resonant Converter for Wide Load Range", M.S. thesis, Virginia Polytechnic Institute and State University, Blacksburg, Virginia, 2007.

[10] Cadar Dorin, Petreus Dorin, Ciocan Ionuț, Dobra Petru, "An Improvement on Empirical Modelling of the Batteries", *The 32nd International Spring Seminar on Electronics Technology*, Brno,

Czech Republic, 2009.
[11] W. Chen, Z. Y. Lu, X. F. Zhang and S. S. Ye, "A Novel ZVS Step-up Push-pull Type Isolated LLC Series Resonant DC-DC Converter for UPS Systems and its Topology Variations", *The 23rd Annual Applied Power Electronics Conference and Exposition*, Austin, pp. 1073-1078, 2008.
[12] B. Yang, F. C. Lee, A. J. Zhang and G. Huang, "LLC Resonant Converter for Front end DC/DC Conversion", *The 23rd Annual Applied Power Electronics Conference and Exposition*, Dallas, pp. 1108–1112, 2002.
[13] I. Batarseh, R. Liu, C. Q. Lee and A. K. Upadhyay, "Theoretical and Experimental Studies of the LCC-type Parallel Resonant Converter," *IEEE Transactions on Power Electronics*, Vol. 5, Issue 2, pp. 140-150, April, 1990.
[14] A. J. Gilbert, C. M. Bingham, D. A. Stone and M. P. Foster, "Normalized Analysis and Design of LCC Resonant Converters", *IEEE Transactions on Power Electronics*, Vol. 22, Issue 6, pp. 2386-240, November 2007.
[16] M. P. Foster, H. I. Sewell, C. M. Bingham, D. A. Stone and D. Howe, "Methodologies for the Design of LCC Voltage-Output Resonant Converters", *Proceedings of the IEEE Electr. Power* Appl., Vol. 153, Issue 4, pp. 559-567, July 2006.
[17] D. Fu, F. C. Lee, Q. Yang and F. Wang, "A Novel High-Power-Density Three-Level LCC Resonant Converter with Constant-Power-Factor-Control for Charging Applications", *IEEE Transactions on Power Electronics*, Vol. 23, Issue 5, pp. 2411-2420, Sept. 2008.